Journal of Materials Chemistry C

ROYAL SOCIETY OF CHEMISTRY

PAPER

View Article Online
View Journal | View Issue

Cite this: *J. Mater. Chem. C*, 2023, **11**, 10884

Columnar liquid-crystalline J-aggregates based on N-core-substituted naphthalene diimides†

Eduardo Castellanos,[a] Rosa María Gomila,[a] Rasitha Manha,[b] Gustavo Fernández,[b] Antonio Frontera *[a] and Bartolomé Soberats *[a]

Received 4th May 2023,
Accepted 1st June 2023

DOI: 10.1039/d3tc01560b

rsc.li/materials-c

We report two distinct approaches to prepare unprecedented liquid-crystalline (LC) J-aggregates based on bis-core-dendronized naphthalene diimides (NDIs). The NDI **1**, with free imidic NH groups, spontanously self-assembles *via* hydrogen bonds into a columnar LC structure where the chromophores organize with the cores parallel to the columnar axis. Quantum mechanics calculations (GFN2-xTB method) and middle angle X-ray scattering confirmed the uncommon columnar architecture for the LC **1** which enable strong J-type exciton coupling between NDI cores. On the other hand, the NDI **2**, with *N*-butyl groups at the imide positions, spontaneously self-assembles by cofacial π–π stacking into columnar H-aggregates; however mechanical shearing of the samples induces the reversible formation of weakly coupled J-aggregates. Surprisingly, this mechanochromic behavior is induced by a molecular reorganization of the NDI cores, which is accompanied by a fluorescence turn on. Thus, in this work we successfully applied two approaches to prepare for the first time LC NDI J-aggregates, which are highly appreciated materials for photonic applications.

Introduction

Naphthalene diimide (NDI) dyes belong to the family of rylene diimides[1–3] and consist of a naphthalene scaffold functionalized with two imide groups at the α positions.[4–6] As a result of their molecular structure, they present good absorption and emission properties along with an outstanding photo- and thermostability, being very versatile in terms of synthetic accessibility and tunability of the photophysical properties.[4–9] Moreover, the self-assembly behaviour of NDIs has attracted considerable attention for the development of functional materials for organic electronics,[10–12] as well as for the preparation of biomimetic membranes,[13] and photo-synthetic systems,[14,15] among others. In particular, several efforts have been focused on the development of functional NDI supramolecular polymers and gels,[16–29] that generally exhibit H-type, and to a much lesser extent, J-type exciton coupling.[26–29] In general, J-aggregates present advantageous absorption and emission properties and long exciton lifetimes, and therefore are ideal candidates for photonic applications.[30–32] One strategy to obtain NDI J-aggregates in solution consists of introducing hydrogen (H-) bonding units in the structure.[26–29] For example, it has been reported that NDI J-aggregation can be achieved using imide and amide groups driving the assembly into fibrillar, tubular and/or nano-tape like architectures, with bright emission properties.[26–29]

Even though NDI-based supramolecular polymers have been widely investigated, it is somehow surprising the scarce examples of NDI liquid crystals existing in bibliography,[33–41] especially compared to its larger parent perylene diimides (PDIs).[42–48] Different molecular designs have been applied to develop liquid-crystalline (LC) NDIs, as for example, using perfluorinated[34,35] or oligodimethylsiloxane lateral chains,[41] amphiphilic systems,[36] or donor–acceptor dyads,[39,40] while the introduction of H-bonding units in the NDI design has been scarcely explored.[33] In all these examples, the NDIs are functionalized with alkyl groups at the imide positions and organize in columnar assemblies by the common co-facial π–π stacking. So far, the preparation of LC NDI J-aggregates has remained elusive; their development would render robust photoactive systems with the anisotropic and stimuli-responsive properties characteristic of liquid crystals,[49–53] making them privileged materials for photonics and smart devices.

Herein, we report the first examples of LC NDI J-aggregates. To this end, we exploited different design strategies using wedge-shaped N-core-substituted NDIs **1** and **2** (Fig. 1a) and H-bonds. NDI-**1**, with free N–H groups at the imide positions, forms a columnar rectangular (Col_r) LC J-aggregate where each column is composed of four H-bonded NDI strands with the

[a] *Department of Chemistry, Universitat de les Illes Balears, Cra. Valldemossa km 7.5, 07122 Palma de Mallorca, Spain. E-mail: toni.frontera@uib.es, b.soberats@uib.es*
[b] *Organisch-Chemisches Institut Westfälische Wilhelms, Universität Münster, Corrensstraße 36, 48149 Münster, Germany*

† Electronic supplementary information (ESI) available: These might include the materials and methods, synthetic procedures, NMR spectra, additional UV/vis experiments, microscopic experiments, DSC, computational details, additional X-ray experiments, *etc.* See DOI: https://doi.org/10.1039/d3tc01560b

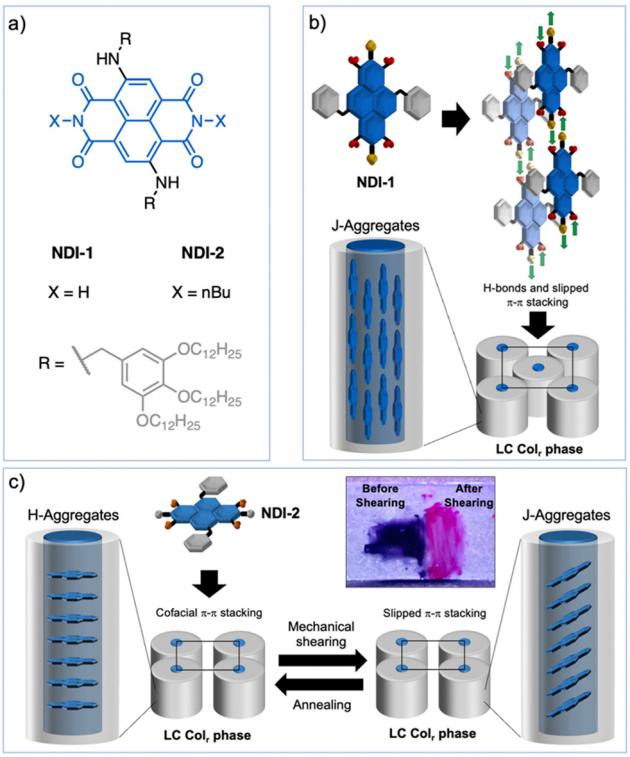

Fig. 1 (a) Molecular structures of NDI **1** and **2**. (b) Self-assembly behaviour of NDI-**1** into columnar LC J-aggregates driven by H-bonds. (c) Self-assembly properties of NDI-**2** forming columnar LC H-aggregates exhibiting mechanochromic behaviour caused by a molecular rearrangement in the columnar structure. Inset shows the fluorescence of an NDI-**2** thin film under UV illumination (λ = 365 nm) before (left) and after (right) shearing.

cores oriented parallel to the columns (Fig. 1b).[44,54–56] This is an unconventional columnar assembly that promotes up to three distinct J-type of exciton couplings between dyes,[30–32] as it was observed using theoretical models. In contrast, NDI-**2** with butyl groups at the imide positions, self-organizes into a columnar LC H-aggregate characterized by the conventional co-facial organization of the dyes along the columns (Fig. 1c). Remarkably, the LC NDI-**2** exhibits a reversible fluorescence turn on upon mechanical shearing, which is triggered by the formation of a J-aggregate *via* an intracolumnar molecular reorganization of the NDIs from face-to-face to slipped NDI interactions (Fig. 1c). This is a new mechanochromism mechanism in liquid crystals, that permitted the transformation of H- to J-aggregates without any phase transition. The newly prepared LC NDIs hold promise as photonic smart materials, while this work discloses sophisticated strategies to develop LC J-aggregates that could be applied to control exciton coupling in dye-based assemblies.

Results and discussion

Molecular design and optical properties of NDIs 1 and 2 in solution

The molecular structures of compounds **1** and **2** are based on NDI scaffolds functionalized with two amino(3,4,5-dodecyloxybenzyl) groups at the 2 and 6 positions of the core. The wedge-shaped groups were expected to provide solubility in organic solvents as well as LC behaviour in bulk. While NDI-**2** carries two butyl groups at the imide positions, the NDI-**1** bears two free NH groups, which were introduced to provide the ability to establish H-bonding interactions, according to previous reports.[25,27] On the other hand, the N-core substitution pattern was selected because it is known to induce a significant decrease of the HOMO–LUMO bandgap with respect to unsubstituted NDIs, leading to systems absorbing between 550 and 650 nm, close to the near infrared region.[7] The NDIs **1** and **2** were synthesized with moderate to good yields by adaptation of previously described synthetic procedures,[8] and were isolated as dark blue waxy solids (ESI,† Fig. S3–S6).

To initially assess the optical features of the new NDIs, we carried out UV/vis studies in chloroform ($CHCl_3$) and methylcyclohexane (MCH) (Fig. 2a and b). NDIs **1** and **2** presented analogous UV/vis profiles in $CHCl_3$ consisting of an intense band with a vibronic progression around 600 nm, and a less intense band around 350 nm. This UV/vis pattern is consistent with other 2,6-amine-core-substituted NDIs in their monomeric state, with a relatively low HOMO–LUMO bandgap and the main absorption band red-shifted with the respect to unsubstituted NDIs.[7] The spectra of both compounds significantly changed in MCH. In the case of NDI-**1**, the UV/vis profile experienced a significant red shift of the most intense band from 600 nm to 670 nm, which is diagnostic of the formation of a J-aggregate as it is also confirmed by fluorescence measurements (Fig. S7 and S8, ESI†).[30–32] The UV/vis profile of NDI-**2** in MCH suggested the formation of a slightly coupled J-aggregate, as it can be deduced

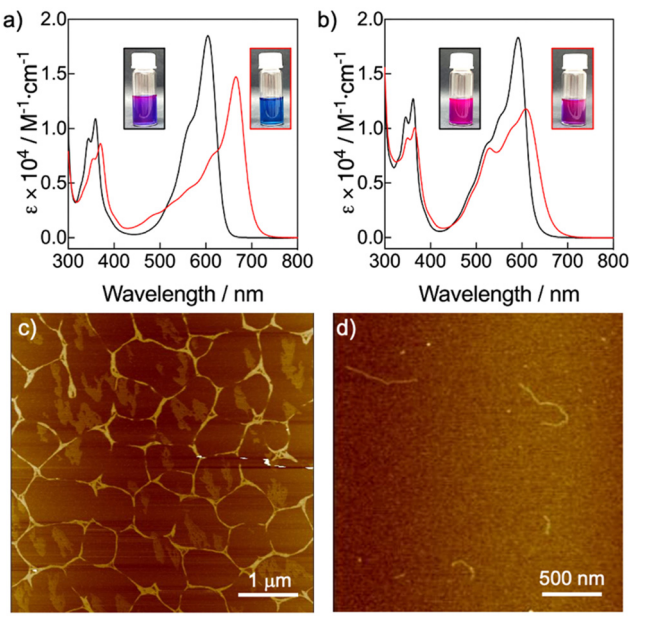

Fig. 2 UV/vis spectra of (a) NDI-**1** (8×10^{-5} M) in $CHCl_3$ (black line) and in MCH (red line); (b) NDI-**2** (5×10^{-5} M) in $CHCl_3$ (black line) and in MCH (red line). Insets show the corresponding-coloured solutions of the samples. AFM images of (c) NDI-**1** (8×10^{-5} M) and (d) NDI-**2** J-aggregate (5×10^{-5} M) spin-coated MCH solutions onto mica substrates.

from the subtle bathochromic shift of the main monomeric band from 590 to 610 nm (Fig. 2b and Fig. S7, ESI†). However, our findings suggest that NDI-**2** concurrently self-assembles into distinct aggregates, one aggregate with an absorption maximum at 550 nm, and a J-aggregate with the absorption maximum at 610 nm (Fig. 2b). This conclusion is supported by the observation that the emission spectra of the NDI-**2** sample change depending on the excitation wavelength (Fig. S9, ESI†), while the confocal microscope images display two distinct emission domains (Fig. S10, ESI†).

To characterize the supramolecular polymerization features of NDIs **1** and **2**, we carried out temperature- and solvent-dependent UV/vis experiments. The variable temperature (VT) experiments of NDI-**1** showed a two-step process that could not be fitted to any aggregation models (Fig. S11, ESI†).[57–59] By a temperature shock experiment, we found that this two-step assembly process was caused by the formation of a kinetically trapped J-type aggregate (λ_{max} = 625 nm) that evolves over time to the thermodynamic and strongly coupled J-aggregate (λ_{max} = 670 nm) (Fig. S12, ESI†). The aggregation mechanism of NDI-**1** under thermodynamic conditions could be studied by a denaturation experiment in MCH and $CHCl_3$ (Fig. S13, ESI†).[60] The non-sigmoidal plot of the fraction of aggregated species (α_{agg}) *vs.* the volume fraction of $CHCl_3$ monitored at 665 nm indicates a cooperative process with a ΔG° of −37.3 kJ mol^{-1} and σ = 0.02 (Table S1, ESI†).[59,60] On the other hand, the aggregation behaviour of NDI-**2** (Fig. 2b) was characterized by a VT UV/vis experiment in MCH (Fig. S14, ESI†). The plot of α_{agg} *vs.* temperature extracted from this experiment was found to fit well to the isodesmic model with a ΔG° of −24.58 kJ mol^{-1} (Table S2, ESI†).[59]

The morphologies of the NDIs **1** and **2** aggregates in MCH were further examined by AFM microscopy upon spin-coating the respective aggregate solutions on mica substrates (Fig. 2c, d and Fig. S15, S16, ESI†). In the case of the NDI-**1**, the AFM images showed long fibrillar structures of 15–17 nm of height (Fig. 2c), which tend to form bundles. The formation of long fibrillar structures is consistent with a cooperative supramolecular polymer.[57–60] On the other hand, AFM images of the NDI-**2** aggregate showed fibrillar assemblies (Fig. 2d) but shorter than those observed for NDI-**1**. The formation of discrete fibers is consistent with a supramolecular polymer formed *via* an isodesmic process.[57–60]

Liquid-crystalline behaviour of NDIs 1 and 2.

The LC properties of the NDI-**1** and NDI-**2** were initially examined by polarizing optical microscopy (POM), differential scanning calorimetry (DSC) and X-ray scattering. Pleasingly, both NDIs showed thermotropic LC properties characterized by a fluidic behaviour and birefringence under cross polarizers. Fig. 3b and c (insets) show the POM images of NDI-**1** and NDI-**2** at 100 and 60 °C, respectively that are compatible with columnar LC phases.[61,62] DSC measurements on NDI-**1** confirmed the formation of an enantiotropic LC phase from 19 °C until 131 °C (cooling cycle), upon which the sample clears (Fig. 3a and Fig. S17, ESI†). Fig. 3b shows the X-ray pattern of NDI-**1** at 100 °C that

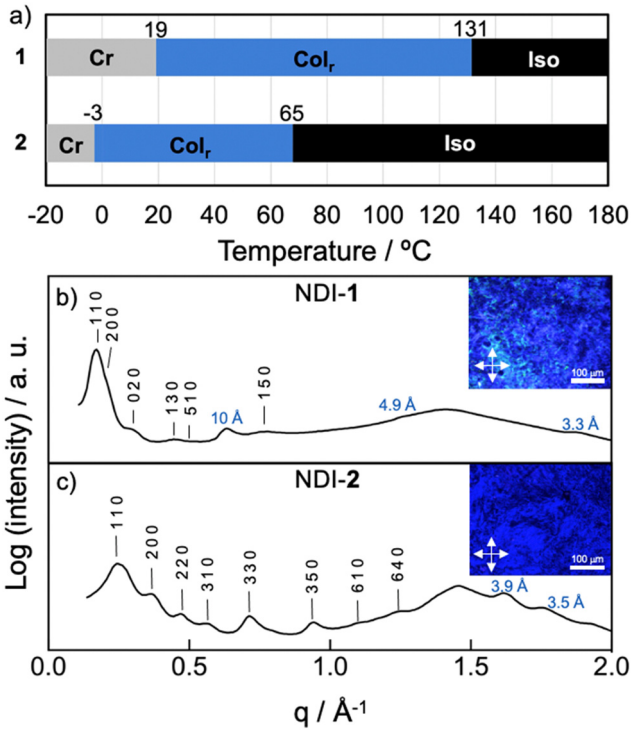

Fig. 3 (a) Temperature-dependent phase transition behaviour of NDIs **1** and **2**. Cr = crystal (according to POM observations); Col$_r$ = columnar rectangular; Iso = isotropic liquid. Phase-transition temperatures were obtained from the first cooling cycle of the DSC curves (Fig. S17 and S18, ESI†) and POM observations. (b) X-ray pattern of NDI-**1** at 100 °C indexed to a LC Col$_r$ phase (a = 60 Å; b = 43 Å). Inset shows the POM image at 100 °C. (c) X-ray pattern of NDI-**2** at 60 °C indexed to a LC Col$_r$ phase (a = 35 Å; b = 41 Å). Inset shows the POM image at 60 °C. Distances displayed in blue correspond to meridional signals (layer lines "L = 1, 2, 3, ...").

exhibits an intense peak at 35 Å with a shoulder at 29.7 Å and a set of weaker peaks at 21.2, 13.9, 11.5, and 8.4 Å which were assigned to the 110, 200, 020, 130, 510 and 150 reflections of a Col$_r$ phase (*p2mm*) with a = 60 Å and b = 43 Å (for further details, see Table S3, ESI†)[63] The diffractogram also showed the diffused halo around 4.5 Å originated from the packing of the long alkyl chains.

On the other hand, the combination of DSC and POM experiments permitted to determine that NDI-**2** displays a LC phase from −3 until 65 °C (Fig. 3a and Fig. S18, ESI†), clearing at lower temperature than NDI-**1**. This large difference in the clearing points is likely caused by the formation of intermolecular H-bonds in NDI-**1**.[64] The X-ray pattern of NDI-**2** at 60 °C showed two intense peaks in the small angle region at 26.4 and 17.3 Å and six weaker peaks distributed along middle and wide-angle region (Fig. 3c). This X-ray pattern was found to match with a Col$_r$ (*c2mm*) lattice with a = 35 Å and b = 41 Å (Table S3, ESI†).[63] The high number of peaks indicate that NDI-**2** exhibited a highly ordered LC phase.

Molecular arrangement of the columnar LC phases of 1 and 2

To gain further details about the molecular arrangement of the Col$_r$ phases, we carried out 2D middle angle X-ray scattering (MAXS) measurements on extruded fibers of NDI-**1** and NDI-**2**

(Fig. 4 and Fig. S19, ESI†). Fig. 4 shows the 2D MAXS pattern of NDI-**1** at 100 °C which clearly evidences the anisotropic features of the aligned sample. The 2D pattern exhibits the main signals ascribed to the Col_r lattice along the equator (Fig. 4), while an intense reflection is observed on the meridian at 10 Å. This distance is consistent with the NDI core length along its long axis (Fig. 5a and Fig. S22, ESI†), and was assigned to layer line $L = 1$. Layer lines $L = 2$ and $L = 3$ also appear along the meridian at 4.9 and 3.3 Å respectively (Fig. 4). The fact that $L = 1$ appeared at 10 Å suggests that the NDI cores are arranged with their long axes parallel to the columnar axis.[44,54–56] Using the Col_r lattice parameters, we calculated the number of molecules per columnar stratum, which was estimated to consist of four NDIs for each 10 Å columnar section (Table S4, ESI†). According to this, NDI-**1** forms a LC columnar assembly where each columnar stratum (10 Å) contains four NDI molecules oriented along the columnar axis (*vide infra*). The absence of off-meridional signals in the 2D MAXS pattern rules out the formation of a helical organization in the system.

To further analyze the arrangement of the molecules in the NDI-**1** Col_r phase, we conducted UV/vis and FT-IR spectroscopy experiments in the solid state. It is noteworthy that the UV/vis profile of NDI-**1** in thin film showed a broad band with the maximum at 660 nm (Fig. S20, ESI†), which indicates that the dye also forms a J-aggregate (Fig. 2a) in LC/solid state. Additionally, we performed polarized UV/vis measurements (Fig. S20, ESI†) on aligned thin films of LC NDI-**1** (Fig. S21, ESI†) that were prepared after mechanical shearing of the sample on a quartz plate (Fig. S21, ESI†). Remarkably, the NDI main absorption band is very intense when the polarizer is oriented parallel to the shearing direction, but the intensity decreases with the polarizer oriented perpendicular (Fig. S20, ESI†). This behavior clearly confirms that the NDI cores are aligned with their molecular long axis (transition dipole moment, Fig. S22, ESI†) parallel to the columnar axis,[44,54] as anticipated from the MAXS experiments. On the other hand, the IR spectra of NDI-**1** (Fig. S23, ESI†) showed two bands at 3300 and 3150 cm^{-1} corresponding to the NH stretching bands (ν_{NH}) of the amine and imidic NHs groups of the molecule, respectively. The low wavenumbers of these bands indicate that both NHs are H-bonded.[44,54] We initially assumed that the naphthalene-NHs (ν_{NH1} = 3300 cm^{-1}) form intramolecular H-bonds with the proximal carbonyl groups (*vide infra*), while the imidic NHs (ν_{NH2} = 3150 cm^{-1}) form intermolecular H-bonds with another NDI (Fig. 1b).[25,27,65] The appearance of two C=O stretching bands at 1660 and 1730 cm^{-1} points towards two distinct H-bonding profiles in the assembled structure (*vide infra*).

Analogous 2D MAXS studies were performed on NDI-**2** (Fig. S19, ESI†). In this case, it was not possible to obtain properly aligned fibers of NDI-**2**, and therefore we could not get a clear anisotropic information of the assembly. Nevertheless, from the MAXS pattern (Fig. S19, ESI†) we could deduce that, in contrast to NDI-**1**, the columnar assemblies of NDI-**2** consist of co-facially assembled molecules. This was deduced from the observation of a strong peak at 3.5 Å along the meridian which is characteristic of the π–π stacking distance in conventional co-facial assemblies.[61,62] No meridional signal at 10 Å was observed in the pattern, ruling out the parallel orientation of the NDI cores along the column. FT-IR (Fig. S24, ESI†) and UV/vis (Fig. S27, ESI†) experiments were also performed on NDI-**2**, which revealed the formation of H-aggregates in the solid state and the establishment of intramolecular H-bonds in the system (ν_{NH1} = 3295 cm^{-1}).[44]

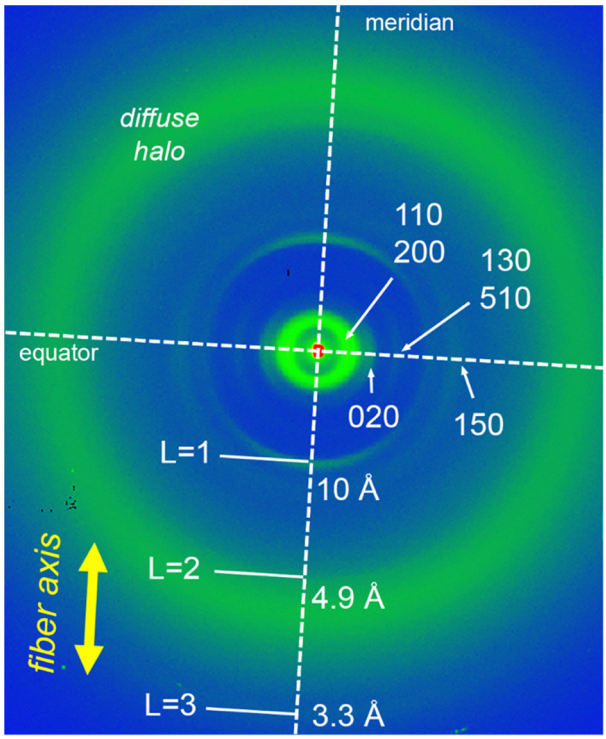

Fig. 4 MAXS diffraction pattern at 100 °C of and aligned fiber of NDI-**1**. The orientation of the fiber is indicated by a yellow arrow and the meridian and equator by white dashed lines. The reflections on the equator are indexed according to a Col_r phase. The reflections of the meridian are indicated as layer lines (L = 1–3).

Theoretical studies

To propose a more detailed self-assembly model of LC NDI-**1**, we carried out theoretical calculations, using as a starting point the experimental results on the X-ray, FT-IR and UV/vis studies. For this purpose, we have used Grimme's extended semiempirical tight-binding method (GFN2-xTB).[66] This computational tool was originally designed for the fast calculation of both covalent structures and supramolecular assemblies with roughly 1000 atoms. It should be emphasized that the model for NDI-**1** and NDI-**2** studied herein are composed of 3584 and 1984 atoms, respectively. The structural models consist of columnar assemblies of the corresponding NDI in the center of the columns, where the surrounding dodecyl chains have been replaced by nonyl chains to keep the calculation doable. The important novelty of the GFN2-xTB method is the utilization of anisotropic second order density fluctuation effects,[66] thus resulting in a more physically sound method compared to standard semiempirical methods. Also important, especially for the systems reported herein, is that the D4 dispersion model is incorporated self-

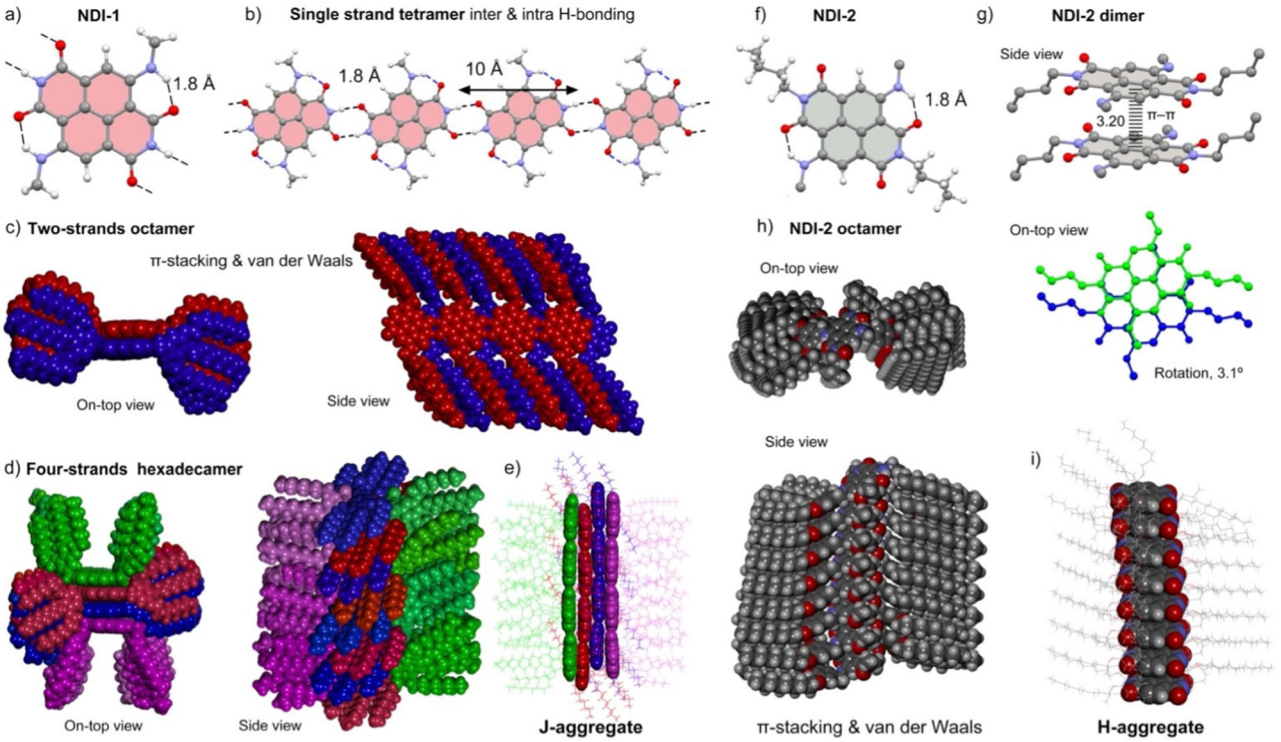

Fig. 5 (a) Optimized geometry of monomeric NDI-**1** (3,4,5-alkyloxybenzyl residues have been omitted). (b) Representation of the one strand and the H-bonds (3,4,5-alkyloxybenzyl residues have been omitted). (c) On-top (left) and side (right) views of two π-stacked strands (octamer), showing the interdigitation of the alkyl chains. (d) On-top (left) and side (right) views of four π-stacked strands (hexadecamer), showing the interdigitation of the alkyl chains in the middle strands and the accommodation of the two external strands. (e) Detail of the J-aggregate that is formed in the four-strand assembly. (f) Optimized geometry of monomeric NDI-**2** (3,4,5-alkyloxybenzyl residues have been omitted). (g) Side (top) and on-top (bottom) views of the π-stacked dimer (3,4,5-alkyloxybenzyl residues have been omitted), showing the π–π distance and a small rotation of 3.1°. (h) On-top (top) and side (bottom) views of the optimized octameric assembly of NDI-**2**. (i) Detail of the H-aggregate that is formed in the columnar assembly of NDI-**2**.

consistently,[67] allowing an adequate description of both π-stacking interactions and van der Waals CH···HC contacts. Both noncovalent forces play a crucial role determining the final architecture of the assemblies, as discussed below.

The complete construction of the columnar assembly of LC **1** is depicted in Fig. 5a–e. The single NDI-**1** forms two intramolecular NH···O H-bonds (Fig. 5a) fixing the conformation of the amino groups at 2 and 6 positions. These H-bonds weaken the ability of these O-atoms to participate in intermolecular H-bonds in comparison to the other two O-atoms, which indeed participate in the intermolecular NH···O H-bonds. NDI-**1** self-assembles forming four symmetrically equivalent H-bonds (1.80 Å) at both ends of the NDI generating the one strand represented in Fig. 5b.[25,27,65] Quite remarkably, these 1D infinite strands can further stack forming two-stranded assemblies, as shown in Fig. 5c. Interestingly, in this assembly, parallel-displaced π-stacking interactions between the NDIs are established. Its formation is likely very favored due to the strong complementarity of the strands and the establishment of the π-stacking and van der Waals interactions between the interdigitated alkyl chains, which in turn determines the degree of displacement between NDI cores (J-aggregates). Additional interdigitation with other strands is not possible since most of the space is occupied by the 3,4,5-alkyloxybenzyl residues (Fig. 5c). Therefore, this two-stranded assembly can only interact with two additional strands, as detailed in Fig. 5d. As can be observed in Fig. 5d, these two strands are U-shaped to fit in the space left upon the π-stacking of the middle strands. Moreover, after the assembly of the outer strands, the volume occupied by the U-shaped 3,4,5-alkyloxybenzyl residues does not allow further growth of the fiber in this direction (additional stacking of strands). It is noteworthy that this four-stranded H-bonded model excludes the generation of helical structures agreeing well with the experimental findings (2D MAXS). Moreover, the simulated 2D X-ray patterns generated with the software CLEARER (Fig. S25, ESI†) matches well with the experimental results, which supports our computational model.

The modelled assembled structure of NDI-**1** (Fig. 5d and e) was utilized to derive the optical properties in solid state by applying the Kasha's exciton theory based on the point-dipole approximation excluding vibronic coupling (ESI,† Tables S5 and S6).[68] Remarkably, the four-stranded structure presents up to three J-type couplings (J_{1-3}) and one H-type coupling (J_4) characterized by the distinct geometrical parameters (center to center distance r, slip angle θ, twist angle α) (Fig. S26, ESI†). For the calculation of the couplings, we utilized the transition dipole moments (μ_{eg}) of the NDI-**1** (4.4 D) determined from the absorption spectrum measured in $CHCl_3$, which provides a consistent value considering the theoretical calculations (Fig. S22, ESI†). It was found that the system presents four relevant J-type contributions with values of $J_1 = -174$ cm^{-1},

$J_2 = -426\ cm^{-1}$, $J_3 = -674\ cm^{-1}$ and $J_4 = +193\ cm^{-1}$ (Table S5, ESI†). These results agree with the UV/vis observations showing a significant bathochromic shift of 1025 cm^{-1} between the monomeric species in solution (maximum at 600 nm) and the solid-state LC J-aggregate (maximum at 660 nm).

On the other hand, GFN2-xTB calculations of the NDI-**2** assembly show that the π-stacking results in a co-facial assembly (Fig. 5f–j) where the distance between the NDI planes is 3.2 Å. Moreover, the molecules are slightly rotated (3.1°) with respect to one another (Fig. 5g). The optimization of the octameric assembly discloses that NDI-**2** propagates through π–π stacking and van der Waals interactions forming a helical assembly, as can be clearly appreciated in the Fig. 5h. Assuming that the columnar assembly was extended, the helical pitch would result in ∼371 Å (116 molecules). Moreover, the optimized geometry revealed a compact arrangement of the long alkyloxy groups, that probably determines the rotation degree and stabilize the whole columnar structure (Fig. 5h and i).

Solid-state photophysical properties and mechanochromic behaviour

In accord with the theoretical studies, the NDI-**2** showed a UV/vis pattern consistent with the formation of a LC H-aggregate with the main absorption band centered at 580 nm, while the monomeric band in chloroform appears at 590 nm (Fig. 6a and Fig. S27, ESI†). This H-aggregate showed a weak emission in its LC state. On the other hand, NDI-**1** exhibited the typical UV/vis pattern of a J-aggregate (Fig. S20, ESI†), validating the X-ray and the theoretical results (Fig. 5a–e). Next, the stimuli-responsive properties of **1** and **2** were examined by applying mechanical forces (rubbing) on the thin films.[53,69–74] While the film of **1** showed no changes, Fig. 6b shows the pictures of the thin films of **2** before and after the application of mechanical force. The images clearly show an emission turn-on with the appearance of a pink colour after shearing. The UV/vis pattern of the thin-film of **2** showed a significant sharpening accompanied with a bathochromic shift of the main absorption band from 580 nm to 640 nm (Fig. 6a). Considering that the HOMO–LUMO transition band of the monomeric NDI-**2** appears at 605 nm in $CHCl_3$ (Fig. 2b), we assumed that the shearing process induced the formation of a weakly coupled J-aggregate, which remained stable for months at ambient conditions. Fluorescence measurements showed that the sheared sample exhibits an emission band at 670 nm, which is three times more intense than the initial emission (without shearing) of the H-aggregate (Fig. 6a). Importantly, this mechanochromic behavior is reversible, and the samples recovered the initial state by heating (annealing) the sample to 50–60 °C and then cooling at r.t. These results indicate that NDI-**2** self-organizes spontaneously into the H-aggregate, while the LC J-aggregate is only achieved after shearing the sample.

The origin of the mechanochromism in **2** was further investigated by X-ray and FT-IR experiments. X-ray measurements of NDI-**2** were carried out in bulk (in not aligned samples) before and after the mechanical shearing, and revealed no significant changes on the X-ray pattern, apart from a slight sharpening of the peaks, and minor displacements of the signals (Fig. S29, ESI†). Indeed, the π–π stacking distance barely changed (from the initial 3.5 Å to 3.6 Å after shearing), discarding drastic changes in the columnar organization and the molecular packing. Additional X-ray experiments before and after annealing the sheared sample (Fig. S30 and S31, ESI†) showed analogous profiles and intensities, which discards the presence of amorphous phases in the two distinct states (Fig. 6). Thus, the mechanochromic behavior is not induced here by a phase transition like in the common LC mechanochromic systems,[53,69–74] and is probably caused by slight changes in the molecular packing in the columnar phase. This characteristic of the NDI-**2** widens the scope of LC mechanochromic materials, since it allows significant absorption and emission changes without significant structural changes.

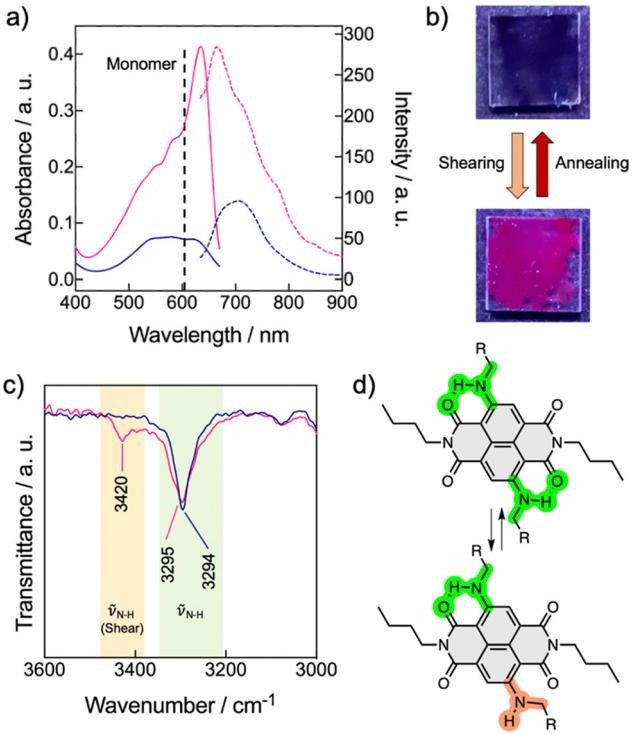

Fig. 6 (a) Absorption (solid line) and emission (dotted line) spectra of NDI-**2** in solid-state before (blue) and after (pink) shearing. Vertical black dotted line indicates the maximum absorption wavelength of the monomer in $CHCl_3$. (b) Thin-film of NDI-**2** (quartz substrate) before (top) and after (down) shearing under UV lamp irradiation (λ = 365 nm). (c) Selected region of the FT-IR spectra of a solid sample of NDI-**2** before (blue) and after (pink) shearing. (d) Proposed conformational changes of the N–H group in NDI-**2** induced by the mechanical shearing.

Interestingly, the FT-IR spectrum of NDI-**2** after shearing revealed the appearance of an additional NH stretching band at 3420 cm^{-1}, coexisting with the original band of the H-bonded N–H (ν_{NH1} = 3295 cm^{-1}) (Fig. 6c and Fig. S24, ESI†). This behavior was attributed to a partial disruption of the intramolecular H-bonds (Fig. 5f), which is probably accompanied by the rotation of the N—naphthalene bond, as shown in Fig. 6d. Thus, it was assumed that the shearing process induced a conformational change in a part of the NDIs of the columnar system, leading to a subtle change in the columnar packing that was enough to

switch from the initial H-type coupling to weakly coupled J-aggregates. We propose that this exciton coupling change was consequence of the subtle tilting of the NDIs cores in the columnar structure, as represented in Fig. 1c. To the best of our knowledge, this is an unprecedented mechanism for a mechanochromic LC system,[53,69–74] which is triggered by a molecular conformational change without an associated phase transition.

Conclusions

We have reported the first examples of columnar LC naphthalene diimide J-aggregates. The NDI-**1** and NDI-**2** consist of N-core-substituted naphthalene diimides and exhibit an intense blue-purple colour. The NDI-**1** was designed to self-assemble *via* quadruple hydrogen bonds into liquid-crystalline columnar assemblies where the dyes are oriented parallel to the columnar axes. Middle angle X-ray scattering, polarized UV/vis spectroscopy and quantum mechanics calculations were utilized to create a model of the NDI-**1** liquid-crystalline assembly and revealed a complex four-stranded columnar packing where the chromophores stablish up to three J-type couplings. The packing of the peripheral alkyl chains was found to be crucial in the assembly and determines the number of strands and the relative position of the naphthalene diimide cores in within the columns. In contrast, NDI-**2** self-assembles into columnar liquid-crystalline H-aggregates, and only forms J-aggregates upon mechanical shearing of the sample. This approach renders stable room temperature J-aggregates, whose emission is turned-on upon application of a mechanical stimulus. Remarkably, the mechanochromism in the liquid-crystalline NDI-**2** is triggered by an unprecedented mechanism entailing the partial disruption of the intramolecular hydrogen bonds and a conformational change in the naphthalene diimide core that in turn leads to a rearrangement of the chromophores in the columnar structure switching from H- to J-type couplings. We believe that these new NDI materials hold great promise for their implementation in photonics and as stimuli-responsive systems. Moreover, this work provides new insights into structure/property correlations for the design of LC J-aggregates, which might be applied in a wide variety of dyes.

Author contributions

Eduardo Castellanos: synthesis, spectroscopic characterization, methodology and writing. Rosa María Gomila: theoretical studies and retrostructural analysis. Rasitha Manha and Gustavo Fernández: design, interpretation and fittings of the aggregation UV/vis studies and writing. Antonio Frontera and Bartolomé Soberats: conceptualization, writing, supervision and funding acquisition.

Conflicts of interest

There are no conflicts to declare.

Acknowledgements

We thank J. Cifre, G. Martorell, J. González and G. Ramis of the Serveis Cientificotènics (SCT) of the UIB for the technical support. We acknowledge M. F. Infante for their contribution in the experiments of supramolecular polymerization of NDI-**1**. We acknowledge the MICINN/AEI of Spain (Projects PID2019-107779GA-I00/AEI/10.13039/501100011033, EQC2018-004206-P, TED2021-130946B-100) and the GOIB (AAEE 116/2017, AP_2021_042) for financial support. B. S. is thankful to the MICINN/AEI for the ''Ramón-y-Cajal'' fellowship (RYC-2017-21789). G. F. and R. M. thank the Deutsche Forschungsgemeinschat (DFG, Sonderforscungsbereich SFB858) for funding.

Notes and references

1 X. Zhan, A. Facchetti, S. Barlow, T. J. Marks, M. A. Ratner, M. R. Wasielewski and S. R. Marder, *Adv. Mater.*, 2011, **23**, 268–284.
2 X. Zhao, Y. Xiong, J. Ma and Z. Yuan, *J. Phys. Chem. A*, 2016, **120**, 7554–7560.
3 L. Chen, C. Li and K. Müllen, *J. Mater. Chem. C*, 2014, **2**, 1938–1956.
4 S. V. Bhosale, C. H. Jani and S. J. Langford, *Chem. Soc. Rev.*, 2008, **37**, 331–342.
5 S. V. Bhosale, M. Al Kobaisi, R. W. Jadhav, P. P. Morajkar, L. A. Jones and S. George, *Chem. Soc. Rev.*, 2021, **50**, 9845–9998.
6 M. Al Kobaisi, S. V. Bhosale, K. Latham, A. M. Raynor and S. V. Bhosale, *Chem. Rev.*, 2016, **116**, 11685–11796.
7 N. Sakai, J. Mareda, E. Vauthey and S. Matile, *Chem. Commun.*, 2010, **46**, 4225–4237.
8 S.-L. Suraru and F. Würthner, *Angew. Chem., Int. Ed.*, 2014, **53**, 7428–7448.
9 S. Maniam, H. F. Higginbotham, T. D. M. Bell and S. J. Langford, *Chem. – Eur. J.*, 2019, **25**, 7044–7057.
10 F. Würthner and M. Stolte, *Chem. Commun.*, 2011, **47**, 5109–5115.
11 A. Nowak-Król, K. Shoyama, M. Stolte and F. Würthner, *Chem. Commun.*, 2018, **54**, 13763–13772.
12 M. Sommer, *J. Mater. Chem. C*, 2014, **2**, 3088–3098.
13 R. E. Dawson, A. Hennig, D. P. Weimann, D. Emery, V. Ravikumar, J. Montenegro, T. Takeuchi, S. Gabutti, M. Mayor, J. Mareda, C. A. Schalley and S. Matile, *Nat. Chem.*, 2010, **2**, 533–538.
14 E. Iengo, G. D. Pantoş, J. K. M. Sanders, M. Orlandi, C. Chiorboli, S. Fracasso and F. Scandola, *Chem. Sci.*, 2011, **2**, 676–685.
15 V. L. Gunderson, A. L. Smeigh, C. H. Kim, D. T. Co and M. R. Wasielewski, *J. Am. Chem. Soc.*, 2012, **134**, 4363–4372.
16 A. Mukherjee and S. Ghosh, *Org. Mater.*, 2021, **3**, 405–416.
17 P. P. N. Syamala, B. Soberats, D. Görl, S. Gekle and F. Würthner, *Chem. Sci.*, 2019, **10**, 9358–9366.
18 A. Sarkar, S. Dhiman, A. Chalishazar and S. J. George, *Angew. Chem., Int. Ed.*, 2017, **56**, 13767–13771.

19 H. Shao and J. R. Parquette, *Chem. Commun.*, 2010, **46**, 4285–4287.
20 D. S. Pal, H. Kar and S. Ghosh, *Chem. Commun.*, 2018, **54**, 928–931.
21 A. Das and S. Ghosh, *Chem. Commun.*, 2016, **52**, 6860–6872.
22 A. Das and S. Ghosh, *Angew. Chem., Int. Ed.*, 2014, **53**, 1092–1097.
23 R. Khamrui, R. N. Manna, P. Rajdev, A. Paul and S. Ghosh, *ACS Appl. Bio Mater.*, 2022, **5**, 5410–5417.
24 A. Das and S. Ghosh, *Chem. Commun.*, 2016, **52**, 6860–6872.
25 C. Thalacker, A. Miura, S. De Feyter, F. C. De Schryver and F. Würthner, *Org. Biomol. Chem.*, 2005, **3**, 414–422.
26 H. Kar, D. W. Gehrig, F. Laquai and S. Ghosh, *Nanoscale*, 2015, **7**, 6729–6736.
27 H. Kar, D. W. Gehrig, N. K. Allampally, G. Fernandez, F. Laquai and S. Ghosh, *Chem. Sci.*, 2016, **7**, 1115–1120.
28 H. Kar and S. Ghosh, *Chem. Commun.*, 2016, **52**, 8818–8821.
29 H. Shao and J. R. Parquette, *Chem. Commun.*, 2010, **46**, 4285–4287.
30 F. Würthner, T. E. Kaiser and C. R. Saha-Möller, *Angew. Chem., Int. Ed.*, 2011, **50**, 3376–3410.
31 S. S. Babu, V. K. Praveen and A. Ajayaghosh, *Chem. Rev.*, 2014, **114**, 1973–2129.
32 N. J. Hestand and F. C. Spano, *Acc. Chem. Res.*, 2017, **50**, 341–350.
33 N. V. Ghule, R. S. Bhosale, S. V. Bhosale, T. Srikanth, N. V. S. Rao and S. V. Bhosale, *ChemistryOpen*, 2018, **7**, 61–67.
34 Y. C. Wu, P. Leowanawat, H. J. Sun, B. E. Partridge, M. Peterca, R. Graf, H. W. Spiess, X. B. Zeng, G. Ungar, C. S. Hsu, P. A. Heiney and V. Percec, *J. Am. Chem. Soc.*, 2015, **137**, 807–819.
35 M.-S. Ho, B. E. Partridge, H.-J. Sun, D. Sahoo, P. Leowanawat, M. Peterca, R. Graf, H. W. Spiess, X. Zeng, G. Ungar, P. A. Heiney, C.-S. Hsu and V. Percec, *ACS Comb. Sci.*, 2016, **18**, 723–739.
36 T. Sakurai, Y. Tsutsui, K. Kato, M. Takata and S. Seki, *J. Mater. Chem. C*, 2016, **4**, 1490–1496.
37 S. Milita, F. Liscio, L. Cowen, M. Cavallini, B. A. Drain, T. Degousée, S. Luong, O. Fenwick, A. Guagliardi, B. C. Schroeder and N. Masciocchi, *J. Mater. Chem. C*, 2020, **8**, 3097–3112.
38 Y. Xiao, X. Su, L. Sosa-Vargas, E. Lacaze, B. Heinrich, B. Donnio, D. Kreher, F. Mathevet and A.-J. Attias, *CrystEngComm*, 2016, **18**, 4787–4798.
39 J. A. Berrocal, R. H. Zha, B. F. M. de Waal, J. A. M. Lugger, M. Lutz and E. W. Meijer, *ACS Nano*, 2017, **11**, 3733–3741.
40 K. D. Thériault, C. L. Radford, G. P. Nagabhushana, D. T. Hogan, V. E. Williams, T. L. Kelly and T. C. Sutherland, *Mater. Adv.*, 2022, **3**, 328–336.
41 M. Ichikawa, Y. Yokota, H.-G. Jeon, G. D. R. Banoukepa, N. Hirata and N. Oguma, *Org. Electron.*, 2013, **14**, 516–522.
42 R. K. Gupta and A. A. Sudhakar, *Langmuir*, 2019, **35**, 2455–2479.
43 F. Würthner, C. R. Saha-Möller, B. Fimmel, S. Ogi, P. Leowanawat and D. Schmidt, *Chem. Rev.*, 2016, **116**, 962–1052.
44 S. Herbst, B. Soberats, P. Leowanawat, M. Lehmann and F. Würthner, *Angew. Chem., Int. Ed.*, 2017, **56**, 2162–2165.
45 D. Görl, B. Soberats, S. Herbst, V. Stepanenko and F. Würthner, *Chem. Sci.*, 2016, **7**, 6786–6790.
46 M. Funahashi, M. Yamaoka, K. Takenami and A. Sonoda, *J. Mater. Chem. C*, 2013, **1**, 7872–7878.
47 C. Roche, H.-J. Sun, P. Leowanawat, F. Araoka, B. E. Partridge, M. Peterca, D. A. Wilson, M. E. Prendergast, P. A. Heiney, R. Graf, H. W. Spiess, X. Zeng, G. Ungar and V. Percec, *Nat. Chem.*, 2016, **8**, 80–89.
48 D. Sahoo, M. Peterca, E. Aqad, B. E. Partridge, P. A. Heiney, R. Graf, H. W. Spiess, X. Zeng and V. Percec, *ACS Nano*, 2017, **11**, 983–991.
49 J. W. Goodby, P. J. Collings, T. Kato, C. Tschierske, H. Gleeson and P. Raynes, *Handbook of Liquid Crystals*, Wiley-VCH, Weinheim, Germany, 2014.
50 T. Kato, M. Yoshio, T. Ichikawa, B. Soberats, H. Ohno and M. Funahashi, *Nat. Rev. Mater.*, 2017, **2**, 17001.
51 T. J. White and D. J. Broer, *Nat. Mater.*, 2015, **14**, 1087–1098.
52 J. Uchida, B. Soberats, M. Gupta and T. Kato, *Adv. Mater.*, 2022, **34**, 2109063.
53 Y. Sagara, S. Yamane, M. Mitani, C. Weder and T. Kato, *Adv. Mater.*, 2016, **28**, 1073–1095.
54 S. Herbst, B. Soberats, P. Leowanawat, M. Stolte, M. Lehmann and F. Würthner, *Nat. Commun.*, 2018, **9**, 2646.
55 B. Soberats, M. Hecht and F. Würthner, *Angew. Chem., Int. Ed.*, 2017, **56**, 10771–10774.
56 M. Hecht, T. Schlossarek, M. Stolte, M. Lehmann and F. Würthner, *Angew. Chem., Int. Ed.*, 2019, **58**, 12979–12983.
57 T. F. A. de Greef, M. M. J. Smulders, M. Wolffs, A. P. H. J. Schenning, R. P. Sijbesma and E. W. Meijer, *Chem. Rev.*, 2009, **109**, 5687–5754.
58 J. Matern, Y. Dorca, L. Sánchez and G. Fernández, *Angew. Chem., Int. Ed.*, 2019, **58**, 16730–16740.
59 M. M. J. Smulders, M. M. L. Nieuwenhuizen, T. F. A. de Greef, P. van der Schoot, A. P. H. J. Schenning and E. W. Meijer, *Chem. – Eur. J.*, 2010, **16**, 362–367.
60 P. A. Korevaar, C. Schaefer, T. F. A. de Greef and E. W. Meijer, *J. Am. Chem. Soc.*, 2012, **134**, 13482–13491.
61 T. Wöhrle, I. Wurzbach, J. Kirres, A. Kostidou, N. Kapernaum, J. Litterscheidt, J. C. Haenle, P. Staffeld, A. Baro, F. Giesselmann and S. Laschat, *Chem. Rev.*, 2016, **116**, 1139–1241.
62 T. Kato, T. Yasuda, Y. Kamikawa and M. Yoshio, *Chem. Commun.*, 2009, 729–739.
63 N. Godbert, A. Crispini, M. Ghedini, M. Carini, F. Chiaravalloti and A. Ferrise, *J. Appl. Cryst.*, 2014, **47**, 668–679.
64 S. Bujosa, E. E. Greciano, M. A. Martínez, L. Sánchez and B. Soberats, *Chem. – Eur. J.*, 2021, **27**, 14282–14286.
65 T. E. Kaiser, V. Stepanenko and F. Würthner, *J. Am. Chem. Soc.*, 2009, **131**, 6719–6732.
66 C. Bannwarth, S. Ehlert and S. Grimme, *J. Chem. Theory Comput.*, 2019, **15**, 1652–1671.
67 E. Caldeweyher, S. Ehlert, A. Hansen, H. Neugebauer, S. Spicher, C. Bannwarth and S. Grimme, *J. Chem. Phys.*, 2019, **150**, 154122.

68 M. Kasha, H. R. Rawls and M. A. El-Bayoumi, *Pure Appl. Chem.*, 1965, **11**, 371–392.
69 Y. Sagara and T. Kato, *Nat. Chem.*, 2009, **1**, 605–610.
70 Y. Sagara and T. Kato, *Angew. Chem., Int. Ed.*, 2011, **50**, 9128–9132.
71 K. P. Gan, M. Yoshio, Y. Sugihara and T. Kato, *Chem. Sci.*, 2018, **9**, 576–585.
72 A. Seki and M. Yoshio, *ChemPhysChem*, 2020, **21**, 328–334.
73 T. Kobayashi, Y. Kitamoto, Y. Hirai, T. Kajitani, T. Seki and S. Yagai, *Commun. Chem.*, 2018, **1**, 58.
74 K. K. Kartha, V. S. Nair, V. K. Praveen, M. Takeuchi and A. Ajayaghosh, *J. Mater. Chem. C*, 2019, **7**, 1292–1297.

